A low-cost and flexible double-crystal monochromator for an x-ray beamline

C. S. Hwang and F. Y. Lin
Synchrotron Radiation Research Center, Hsinchu Science-Based Industrial Park, Hsinchu 30077, Taiwan

Chih-Hao Lee and Kuan-Li Yu
Department of Engineering and System Science, National Tsing Hua University, Hsinchu 30043, Taiwan

C. H. Hsieh
Department of Physics, National Taiwan Normal University, Taipei, Taiwan

P. K. Tseng and J. T. Lin
Department of Physics, Tamkang University, Tamsui, Taipei, Taiwan and Department of Physics, National Taiwan University, Taipei, Taiwan

W. F. Pong
Department of Physics, Tamkang University, Tamsui, Taipei, Taiwan

This work designs and implements an inexpensive and simple double-crystal monochromator, which yields a high performance at a bending magnet x-ray beamline. A primary feature of the proposed monochromator is that the offset between the incident and monochromatic exit of the x-ray beam can be adjusted to cover a wide energy range with a short $X-Y$ traveling stroke. Such a short range of $X-Y$ strokes can reduce the monochromator's overall size and, also, increase the stability of motions. Meanwhile, in this monochromator, instead of using a complicated hardware linkage mechanism, a software program is developed to effectively control the $X-Y$ stage for positioning the second crystal in a fixed exit configuration, alleviating mechanic motion errors to maintain the parallelism of the two crystals. The entire software control mechanical linkage offers a relatively inexpensive and simple assembly monochromator that is more flexible than the commercially available one. © *1998 American Institute of Physics.* [S0034-6748(98)00403-1]

I. INTRODUCTION

The efforts of establishing a synchrotron x-ray beamline by a small research group have received increasing emphasis. Meanwhile, many investigators of the small Participate Research Team (PRT) desire to propose an x-ray beamline to be installed at the Synchrotron Radiation Research Center (SRRC). Although many different kinds of double-crystal monochromators[1–14] have been developed and some of them are commercially available, they are extremely expensive and have some application limitations. These commercial monochromators are ultra-high-vacuum (UHV) compatible in order to extend the lower photon energy range (about 1 keV) of soft x ray and water cooling on the first crystal to ultimately remove the heating load. Typically, these commercial monochromators of the x-ray beamline need an expert manufacturer to perform the high-precision machining for obtaining the high-precision mechanism. Such a monochromator should be extremely expensive, not easier to assemble. In addition, there are very few manufacturers in the world that have the capability to fabricate the high performance of the DCM. Therefore, our design concept can allow everyone to easily assemble a high-performance DCM. Consequently, this DCM reduces cost, is easily maintained, and enhances the flexibility of a monochromator.

A relatively simple and flexible function DCM was recently designed and installed on the B 15B multipurpose x-ray beamline[15] at SRRC. The B 15B beamline is used for experiments involving x-ray spectroscopy, x-ray diffraction, scattering, and instrument development. This DCM attempts to reduce the complexity of the monochromator mechanism, eliminate the nonessential component in the monochromator, simplify the design to reduce costs, and enhance the flexibility to fulfill the minimum requirement of the research members' multipurpose goals. This relatively simple and flexible DCM design contains several unique features:

(1) The DCM is assembled using commercially available components without any difficulty in assembly and maintenance.
(2) All driven mechanisms are controlled by a software program without complicated linkage on the DCM.
(3) The offset between the incident and exit beam can be adjusted by a software program to cover a wide energy range with a short $X-Y$ traveling stroke.
(4) The $X-Y$ translation can be maintained constant while rotating the two parallel crystals for an x-ray absorption near-edge structure (XANES) experiment.
(5) The first crystal can be moved away from the center beam for the white beam experiments.
(6) No water cooling is installed for the first crystal; instead, a backfilled helium cooling is used.

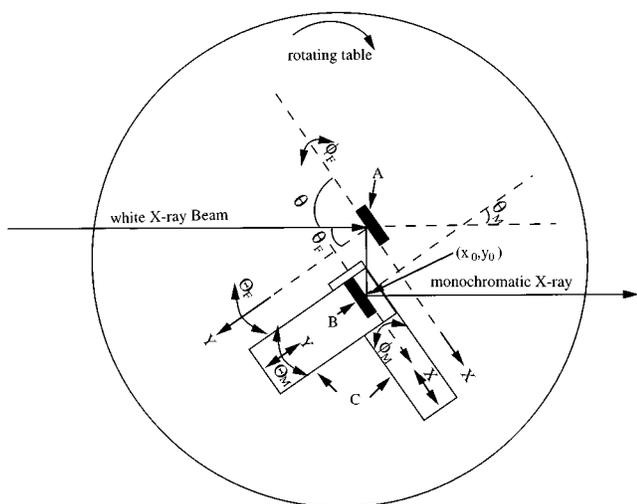This design reduces the overall monochromator size

FIG. 1. An adjustable offset double-crystal monochromator whose $X-Y$ stage was used to position the moving crystal to maintain the exit beam position fixed, where θ_F and θ_M denote the Bragg's angle of the fixed and moving crystal, respectively. In addition, ϕ_F and ϕ_M represent the rotation angle around the x axis and Θ_F and Θ_M are the angle rotation around the y axis. The center of the $X-Y$ stage is at (X_0, Y_0), where A, B, and C denote the fixed and moving crystal, and the $X-Y$ table, respectively.

while still covering a wide energy range without changing the crystals. The following sections will describe the above features. In the future, several monochromators could be installed on the x-ray beamlines at SRRC's bending magnet beam port. This DCM is designed in such a manner to demonstrate that a simple effort can yield a high-performance and flexible monochromator.

II. THE DESIGN FEATURES

This DCM design resembles the most current DCM designs with two identical crystals in parallel.[1–14] Figure 1 schematically depicts the monochromator's mechanism. Two crystals are mounted on the common precision rotating stage. The first crystal (i.e., fixed crystal) is located on the center of the rotating stage and the second one (i.e., moving crystal) is mounted on a two linear $X-Y$ stage, which is also assembled on the same rotation stage. The fixed crystal accepts the incident white x-ray beam and the moving crystal diffracts the beam from the first crystal toward the same direction as the incident beam. To maintain a constant offset distance during the energy scan, the $X-Y$ table must be properly moved during the rotation of the fixed crystal. If there are no pitch, yaw, and roll errors during the motion of the $X-Y$ stage, the surface plane of the moving crystal on the $X-Y$ table can be maintained exactly parallel with respect to the fixed crystal. However, errors arose. For instance, the angle error of $\Delta\theta = \theta_M - \theta_F$ of the moving crystal slightly slips away from the Bragg's condition, and the angle error of $\Delta\phi = \phi_M - \phi_F$ changes the exit beam's horizontal position. Therefore, in this work, two additional stepping motors with a gear reducer are attached to the crystal mount of the moving crystal on the $X-Y$ table. In doing so, θ_M and ϕ_M of the moving crystal can be automatically adjusted in the real-time mode (Fig. 1). Consequently, the errors of pitch $\Delta\theta$ and roll $\Delta\phi$

between the two crystals during the motion of the $X-Y$ stage can be reduced and implement an automatic feedback system.[16–18]

Several design concepts are considered herein to reduce the construction cost and increase the flexibility and precision of the DCM. Such considerations include shortening the traveling stroke of the $X-Y$ stage, as well as eliminating any hardware linkage, non-ultra-high-vacuum compatibility and no water cooling for the first crystal. In addition, this DCM can be operated at a constant offset mode. The offset can also be easily varied by the software control. The offset is adjusted to keep the traveling stroke of the $X-Y$ stage as short as possible. The shorter traveling stroke of the DCM can significantly reduce the monochromator's overall size and ensure adequate stability by maintaining the two crystals in parallel. For instance, in an extended x-ray absorption fine-structure (EXAFS) experiment, a small offset distance can be used in scanning the high-energy range, thereby reducing the distance between the two crystals and the traveling strokes of the $X-Y$ stage. While scanning at low-energy ranges, the offset distance should become large enough to avert the two crystal holders from colliding. Therefore, adjusting the offset distance can shorten the traveling strokes of the $X-Y$ stages and still maintain a wide and useful energy range. In contrast, most monochromators adopt a complicated hardware linkage to maintain a fixed offset without the flexibility of adjusting the offset distance. They must also use a long arm either to position the second crystal or to change crystals with a smaller lattice spacing. In our offset adjustable design, one set of crystals can extend a large energy range. Based on these design concepts, the energy range of this monochromator can be operated from 2 to 29 keV without changing the monochromator crystals Ge(111).

Another means of obtaining the flexible DCM entails removing the complicated machining mechanic linkage for a fixed exit design and, then, replacing it with an all software control linkage through the computer control. In this manner, this DCM's cost and complexity are reduced and its operational flexibility is ultimately enhanced. Under the simple mechanical movement, the mechanical errors in pitch, roll, and yaw can be eliminated by inputting, in advance, the calibrated data of position and angle errors by inserting them into the software to correct the angle error in real time. As long as the mechanical precision is reproducible, the errors of the mechanical motion can be reduced as much as possible by this calibration compensation. Therefore, before mounting the monochromator on the beam line, the departure of θ_M and ϕ_M should be measured and adjusted with respect to θ_F and ϕ_F. Table I indicates that those parameters slightly differ during parallel motion. In this monochromator, the precision of the $X-Y$ stage has been checked, demonstrating that the roll error $\Delta\phi$ and pitch error $\Delta\theta$ in the entire energy scan (θ from 10° to 80°) are less than 10 arc sec, and less than 3 arc sec in the short energy range (θ from 15° to 50°). This is achieved even without implementing any software correction of prealignment correcting factors. Actually, the major corrections of these fine-tuned pitch and roll errors are attributed to the miscutting of monochromator crystals. Each set of monochromator crystals possesses different

TABLE I. Design parameters and performance of the double-crystal monochromator.

Energy scan range	2.0–28.0 keV
Total strokes of $x-y$ table	50 mm
Pitch θ and Roll ϕ precision of $x-y$ table	$<5''$
Angular resolution of θ, ϕ, $\Delta\theta$, and $\Delta\phi$	$0.1''$
Position resolution of $x-y$ table	1 μm
Offset distance range D	7–30 mm
Precision of Bragg angle and its home position	$\pm 2''$
Precision of $x-y$ table and its home position	1 μm
Vacuum system	<0.001 Torr
Range of $\Delta\theta$ and $\Delta\phi$	$\pm 2°$
θ scan range	$3°-75°$
Crystal holder width W	30 mm

precalibration correction values. A manual microscrew knob is also located on the fixed crystal holder to adjust the angle of ϕ, which is essential to compensate the miscutting of the fixed crystal. Table I lists the overall design parameters and performance of the monochromator mechanism. This type of DCM is used herein because the precise computer controlled rotation stage (Kohzu Seiki Co., Japan) and $X-Y$ table (Kohzu Seiki Co., Japan) are commercially available.

In a typical XANES experiment where the scanning energy range is small, the position change of the exit beam is extremely small. Therefore, the XANES experiment can be performed by rotating the entire rotating stage without moving the $X-Y$ stage of the moving crystal. The parallelism of the two crystals can be easily maintained without any motion of the $X-Y$ stage. The position change of the exit beam Δy can be calculated by the relation $\Delta y = D \sin(\theta - \Delta\theta)$ (where $\Delta\theta$ corresponds to the scan energy range ΔE). Figure 2 summarizes the calculation results of the vertical displacement Δy as a function of near-edge energies with different offset D. For instance, when the scan energy range is 100 eV around the 5 keV edge, by using crystal Ge(111) and an offset distance of 10 mm, the position change Δy of the exit beam is within 0.1 mm. The position change becomes even smaller or even negligible when operated at a high-energy range with only a slight offset.
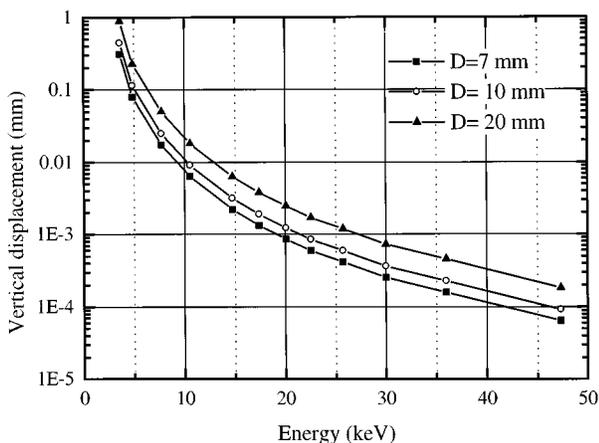

FIG. 2. The exit beam position variation as a function of energy in different offset distances $D=7$, 10, and 20 mm. The $X-Y$ stage does not move during the XANES experiment.
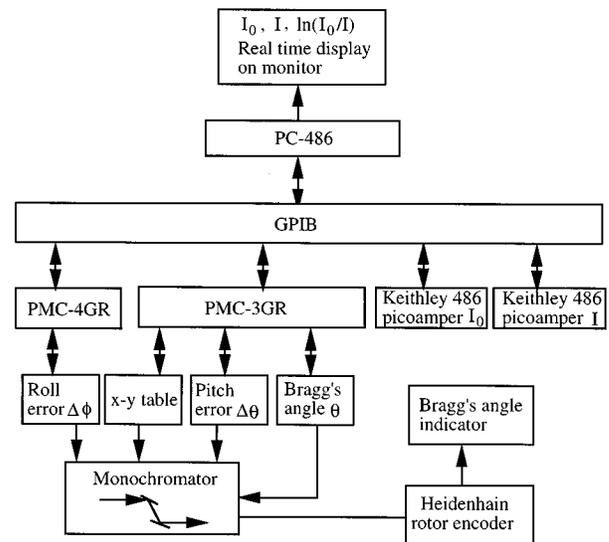

FIG. 3. The hardware architecture of the control and data acquisition system.

The DCM is operated at 1 mTorr of pressure and without water cooling for the first crystal. Two upstream 120 μm Be windows separate the beam-line vacuum from the vacuum of the storage ring, thereby allowing the beam line to operate at a low vacuum or else be backfilled with helium gas. The SRRC electron storage ring is operated at 1.5 GeV (critical energy is 2.2 keV) and these Be windows will reduce the photon flux of the low-energy range of the soft x ray (below 3 keV). Therefore, the thermal load on the first crystal is not a crucial problem. In general, backfilling the vacuum chamber can adequately remove the synchrotron radiation heating on the first crystal. Actually, even without any cooling mechanism and the vacuum operated at 1 mTorr, the DCM can still run a high resolution of XANES spectrum without any difficulty. Notably, implementing a low vacuum environment and noncooling system simplifies the monochromator construction and significantly reduces the cost. In fact, it also increases the mechanical motions' operating stability. Placing several stepping motors inside the vacuum chamber reduces the complexity of the bellows and coupling problem. The restriction of the water/vacuum joint on every cooling channel is also eliminated. In addition, the flexible copper braids do not need to be connected. The non-UHV conditions allow us to quickly replace any parts inside the DCM (including crystals), reducing the maintenance load tremendously.

Figure 3 displays the hardware architecture of the control and data acquisition system. The control system of the software was written in the LABVIEW language on a PC. The stepping controllers (PMC-4GR and PMC-3GR, also from the Kohzu Seiki Co.) control and perform an adjustment on the motions of the $X-Y$ table, Bragg's angle θ, pitch error $\Delta\theta$, and the roll error $\Delta\phi$ of the moving crystal. The home and limit switches are used to automatically set the absolute and limited positions. A Heidenhain rotator encoder is also available to monitor the Bragg's angle, which should be consistent with the angle θ on the PMC-4GR counter. The in-
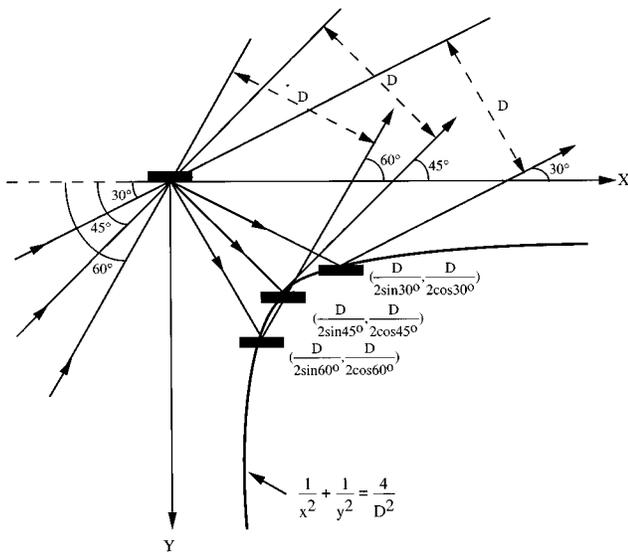
FIG. 4. The trajectory of the moving coordinate (X,Y) during the ''theta scan'' with constant offset distance D. The trajectories of the moving crystal were shown for theta equal to 30°, 45°, and 60°.
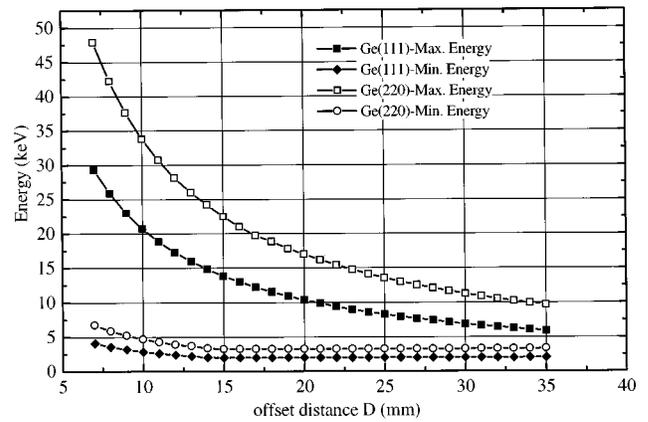

FIG. 5. The relationship between the upper and lower limit in the scanning energy range and the offset distance (D) for crystals of Ge(111) and Ge(220). Assume that θ ranges from 3° to 75° and the stroke of the $X-Y$ stage remains fixed at 50 mm.

tensities of I_0 and I are taken simultaneously to minimize the glitches during the energy scan. Moreover, the intensities of I_0, I, and $\ln(I/I_0)$ are displayed on the PC monitor in real time.

III. OPERATION PRINCIPLES FOR THE DCM

The principle of motion is clarified in the following, particularly when using a software program to control the DCM's motion in a personal computer. Herein, we define a Cartesian coordinate, which is attached to the rotating table and the origin is at the center of the fixed crystal's surface, as shown in Figs. 1 and 4. The moving crystal's position in this coordinate (X,Y) is

$$X = \frac{D}{2 \sin \theta}, \tag{1}$$

$$Y = \frac{D}{2 \cos \theta}, \tag{2}$$

where D denotes the offset distance and θ represents the Bragg's angle. The monochromatic x ray in wavelength λ is diffracted according to Bragg's law

$$n\lambda = 2d \sin \theta, \tag{3}$$

where n and λ denote the order and wavelength of the diffracted monochromatic x-ray beam, respectively. Figure 1 depicts the X and Y coordinates of the moving crystal and the trace of the x-ray beams. This diffracted x-ray beam hits the moving crystal if the moving crystal is on the position (X,Y), as defined by Eqs. (1) and (2). To fix the constant beam exit and maintain a constant offset distance D, the moving crystal trajectory should adhere to the following equation:

$$1/X^2 + 1/Y^2 = 4/D^2. \tag{4}$$

Figure 4 also contains the moving crystal's trajectory on the rotating table. For each movement of the rotating table for different energy scans, the $X-Y$ table depends on the trajectory of Eq. (4) to move the moving crystal. Subsequently, the exit beam will maintain a constant offset distance D (Fig. 4). In addition, data I_0 and I are automatically stored into a data file for further treatment.

IV. THE RANGE OF THE ENERGY SCAN

Strokes S_x and S_y of the $X-Y$ table, the offset distance D, the initial location (X_0,Y_0) of the moving crystal, and the crystal holder width W subsequently limit the scanning energy range of the monochromator (see Table I). Herein, X_0 and Y_0 are defined such that the moving crystal moves from (X_0,Y_0) to (X_0+S_x, Y_0+S_y). Therefore, one can depend on Eqs. (7) and (8) to design the $X-Y$ table strokes. The optimized strokes S_x and S_y of the $X-Y$ table were found to have the following relation:

$$X_0 + S_x = X_{max} = \frac{D}{2} \left(\frac{1}{\sin \theta_{min}} \right), \tag{5}$$

$$X_0 = X_{min} = \frac{D}{2} \left(\frac{1}{\sin \theta_{max}} \right), \tag{6}$$

$$S_x = X_{max} - X_{min} = \frac{D}{2} \left(\frac{1}{\sin \theta_{min}} - \frac{1}{\sin \theta_{max}} \right). \tag{7}$$

The same reason applies for S_y:

$$S_y = \frac{D}{2} \left(\frac{1}{\cos \theta_{max}} - \frac{1}{\cos \theta_{min}} \right). \tag{8}$$

The monochromator used herein is equipped with an $X-Y$ stage with equal strokes $S_x = S_y = 50$ mm, which can adequately cover a wide energy range. However, the actual allowed traveling stroke of the $X-Y$ stage is limited by θ (which also defines the energy) and the offset distance D. For instance, the energy range of the monochromator with the Ge(111) crystals is limited from 4.1 to 29 keV for $D = 7$ mm, and 1.8 to 10.3 keV for $D = 20$ mm. Figure 5 displays the relationship between the offset distance and scan-
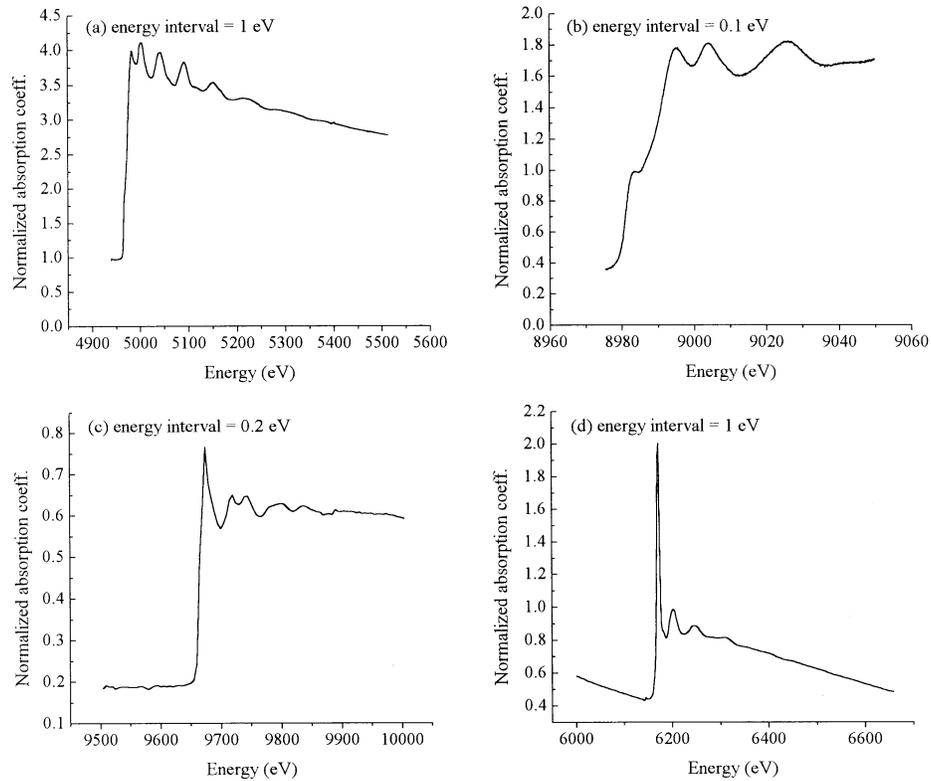
FIG. 6. The x-ray absorption spectrum of (a) Ti foil, (b) the near-edge structure of copper foil, (c) zinc foil, and (d) Nd L_{III} edge of Nd_2O_3 powder.

ning with θ between 3.8° and 75° and $X-Y$ stroke between 0 and 50 mm. The upper limit of the scanning energy is, typically, limited by the maximum stroke of the $X-Y$ stage, which also limits the θ_{min}. Another factor determined θ_{min}, as shown in Eq. (9),

$$\theta_{min} \geqslant \sin^{-1}\left(\frac{S}{W}\right), \qquad (9)$$

where W denotes the crystal holder width and S represents the photon beam size. If $\theta < \theta_{min}$ with certain incidence photon beam size S, part of the direct beam passes through the downstream ion chamber detector (I detector). In addition, the lower limit of the scanning energy is determined by the width of the crystal holder and the offset distance of the incident and exit beam, where θ_{max} is defined in Eq. (10) and keeps $\theta > \theta_{max}$ to prevent the crystal holder from blocking the incidence beam.

$$\theta_{max} \leqslant \cos^{-1}\left(\frac{2 \cdot D}{W}\right). \qquad (10)$$

To obtain the lowest energy, either D must be increased or W must be reduced. However, a small W decreases the throughput of flux at a high energy. Therefore, any energy range cannot be covered without changing either the D distance or the crystals. In our monochromator design, the D distance can be changed by a software program. The program can be set to run the monochromator at a high-energy range with small D and low-energy range with large D without replacing the crystals. The design of this monochromator
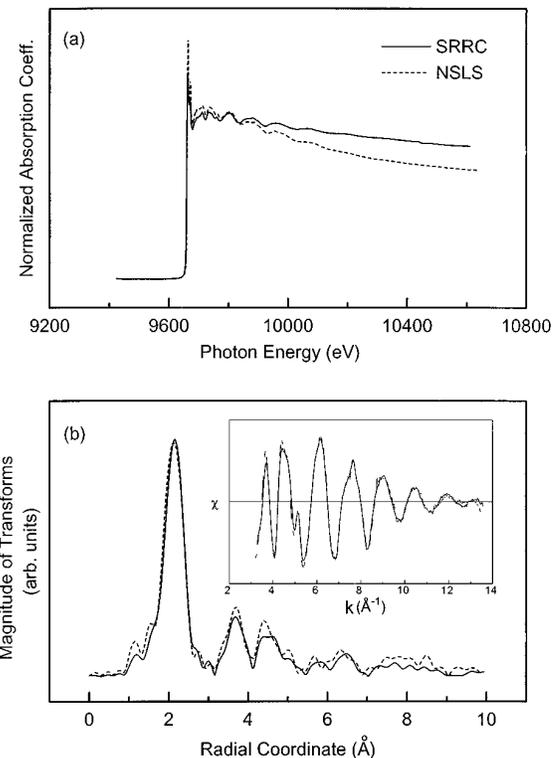

FIG. 7. (a) Normalized Zn K-edge x-ray absorption spectrum of ZnSe, which was measured at the SRRC (solid line) and NSLS-X11-A2 (dashed line) beam lines, respectively. (b) The corresponding magnitude of the Fourier transform of the EXAFS $k^3\chi$ data. The inset represents the Zn K-edge EXAFS oscillations $\chi(k)$ data.

offers a flexible and wide energy range, which most current monochromators with a fixed D distance cannot achieve.

V. EXPERIMENTAL RESULTS

Herein, we measure the absorption spectra of Nd_2O_3, Ti, Cu, and Zn. The Nd_2O_3 sample is a powdered sample pasted on Scotch tape. Other samples come from a commercial EXAFS standard absorber kit (EXAFS Materials Co.). Figures 6(a)–6(d) present the x-ray absorption spectra measurements of Ti, Cu, Zn, and Nd_2O_3 on this monochromator. The expanded K-edge spectrum of copper in Fig. 6(b) clearly demonstrates that the DCM's resolution is satisfactory and sufficient for the edge spectrum.

A sample of ZnSe was measured at the SRRC B15B and National Synchrotron Light Source (NSLS) X11-A2 beamlines,[19] respectively. The spectrum measurement result of the same sample at the two different monochromators demonstrates that the absorption spectrum is quite consistent. This Figure 7 also reveals an adequate resolution of the radial coordinate function of the sample by Fourier transform of the EXAFS analysis. This finding demonstrates that the local structure between atoms can be successfully obtained. The Zn K-edge EXAFS oscillations $\chi(k)$ of our monochromator are also quite consistent with the monochromator of the NSLS. Therefore, these measurement and analysis results of the sample verify that this simple and flexible monochromator can yield a performance as high as the commercially available monochromator.

[1] D. M. Mills, C. Henderson, and B. W. Batterman, Nucl. Instrum. Methods Phys. Res. A **246**, 356 (1986).

[2] A. Habenschuss, G. E. Ice, C. J. Sparks, and R. A. Neiser, Nucl. Instrum. Methods Phys. Res. A **266**, 215 (1988).

[3] H. Kawata and M. Ando, Nucl. Instrum. Methods Phys. Res. A **246**, 369 (1986).

[4] G. Rosenbaum, L. Rock, M. Sullivan, and S. Khalid, Nucl. Instrum. Methods Phys. Res. A **266**, 475 (1988).

[5] M. Lemmonier, O. Collet, C. Depautex, J. M. Esteva, and D. Raoux, Nucl. Instrum. Methods Phys. Res. A **152**, 109 (1978).

[6] J. Goulon, M. Lemmonier, R. Cortes, A. Retourmard, and D. Raoux, Nucl. Instrum. Methods Phys. Res. A **208**, 625 (1983).

[7] T. Matsushita, T. Ishikawa, and H. Oyanagi, Nucl. Instrum. Methods Phys. Res. A **246**, 377 (1986).

[8] J. A. Golovchenko, R. A. Levesque, and P. L. Cowan, Rev. Sci. Instrum. **52**, 509 (1981).

[9] J. P. Kirkland, Nucl. Instrum. Methods Phys. Res. A **291**, 185 (1990).

[10] P. L. Cowan, J. B. Hastings, T. Jach, and J. P. Kirkland, Nucl. Instrum. Methods Phys. Res. A **208**, 349 (1983).

[11] T. Mutata and T. Matsukawa *et al.*, Rev. Sci. Instrum. **63**, 1309 (1992).

[12] M. J. Van Der Hoek, W. Werner, and P. van Zrylen, Nucl. Instrum. Methods Phys. Res. A **246**, 190 (1986).

[13] B. X. Yang, F. H. Middleton, B. G. Olsson, G. M. Bancroft, J. M. Chen, T. K. Shan, K. Tan, and J. Wallace, Rev. Sci. Instrum. **63**, 1355 (1992).

[14] M. Lemonnier, O. Collet, C. Depautex, J. M. Gstena, and D. Redaux, Nucl. Instrum. Methods Phys. Res. A **152**, 109 (1978).

[15] C. H. Lee *et al.*, "The commissioning of a low cost x-ray beam line at SRRC," Presented in the 6th International Conference on Synchrotron Radiation Instrumentation (SRI'97), Himeji, Japan, Aug. 4–8, 1997.

[16] D. Mills and V. Pollock, Rev. Sci. Instrum. **51**, 509 (1980).

[17] M. Ramanathan, M. Engbretson, and P. A. Moniano, Nucl. Instrum. Methods Phys. Res. A **266**, 471 (1988).

[18] A. Krolzig and G. Materlik, M. Suars, and J. Zegnhagen, Nucl. Instrum. Methods Phys. Res. A. **219**, 430 (1984).

[19] W. F. Pong, Ph.D. thesis, University of Notre Dame, IN (1990).